NASA/TM—2016-219074 (Corrected Copy)

A Dual-Plane PIV Study of Turbulent Heat Transfer Flows

Mark P. Wernet and Adam C. Wroblewski
Glenn Research Center, Cleveland, Ohio

Randy J. Locke
Vantage Partners, LLC, Brook Park, Ohio

Corrected Copy issued May 2017.

March 2016

NASA STI Program . . . in Profile

Since its founding, NASA has been dedicated to the advancement of aeronautics and space science. The NASA Scientific and Technical Information (STI) Program plays a key part in helping NASA maintain this important role.

The NASA STI Program operates under the auspices of the Agency Chief Information Officer. It collects, organizes, provides for archiving, and disseminates NASA's STI. The NASA STI Program provides access to the NASA Technical Report Server—Registered (NTRS Reg) and NASA Technical Report Server—Public (NTRS) thus providing one of the largest collections of aeronautical and space science STI in the world. Results are published in both non-NASA channels and by NASA in the NASA STI Report Series, which includes the following report types:

- TECHNICAL PUBLICATION. Reports of completed research or a major significant phase of research that present the results of NASA programs and include extensive data or theoretical analysis. Includes compilations of significant scientific and technical data and information deemed to be of continuing reference value. NASA counter-part of peer-reviewed formal professional papers, but has less stringent limitations on manuscript length and extent of graphic presentations.

- TECHNICAL MEMORANDUM. Scientific and technical findings that are preliminary or of specialized interest, e.g., "quick-release" reports, working papers, and bibliographies that contain minimal annotation. Does not contain extensive analysis.

- CONTRACTOR REPORT. Scientific and technical findings by NASA-sponsored contractors and grantees.

- CONFERENCE PUBLICATION. Collected papers from scientific and technical conferences, symposia, seminars, or other meetings sponsored or co-sponsored by NASA.

- SPECIAL PUBLICATION. Scientific, technical, or historical information from NASA programs, projects, and missions, often concerned with subjects having substantial public interest.

- TECHNICAL TRANSLATION. English-language translations of foreign scientific and technical material pertinent to NASA's mission.

For more information about the NASA STI program, see the following:

- Access the NASA STI program home page at http://www.sti.nasa.gov

- E-mail your question to help@sti.nasa.gov

- Fax your question to the NASA STI Information Desk at 757-864-6500

- Telephone the NASA STI Information Desk at 757-864-9658

- Write to:
  NASA STI Program
  Mail Stop 148
  NASA Langley Research Center
  Hampton, VA 23681-2199

NASA/TM—2016-219074 (Corrected Copy)

A Dual-Plane PIV Study of Turbulent Heat Transfer Flows

Mark P. Wernet and Adam C. Wroblewski
Glenn Research Center, Cleveland, Ohio

Randy J. Locke
Vantage Partners, LLC, Brook Park, Ohio

Corrected Copy issued May 2017.

National Aeronautics and
Space Administration

Glenn Research Center
Cleveland, Ohio 44135

March 2016

Acknowledgments

The authors would like to thank Doug Thurman and Phil Poinsatte for the use of their facility and their support in operating the thin film cooling tunnel. We would also like to thank Garrett Clayo for his assistance in setting up and installing the Dual-Plane PIV system in the thin film cooling rig.

This work was sponsored by the Fundamental Aeronautics Program at the NASA Glenn Research Center.

Level of Review: This material has been technically reviewed by technical management.

Available from

NASA STI Program
Mail Stop 148
NASA Langley Research Center
Hampton, VA 23681-2199

National Technical Information Service
5285 Port Royal Road
Springfield, VA 22161
703-605-6000

This report is available in electronic form at http://www.sti.nasa.gov/ and http://ntrs.nasa.gov/

Corrected Copy

Issued May 2017 for

NASA/TM—2016-219074
A Dual-Plane PIV Study of Turbulent Heat Transfer Flows
Mark P. Wernet, Adam C. Wroblewski, and Randy J. Locke

March 2016

Text, figures, and tables have been changed throughout the report.

A Dual-Plane PIV Study of Turbulent Heat Transfer Flows

Mark P. Wernet and Adam C. Wroblewski
National Aerospace Space Administration
Glenn Research Center
Cleveland, Ohio 44135

Randy J. Locke
Vantage Partners, LLC
Brook Park, Ohio 44142

Abstract

Thin film cooling is a widely used technique in turbomachinery and rocket propulsion applications, where cool injection air protects a surface from hot combustion gases. The injected air typically has a different velocity and temperature from the free stream combustion flow, yielding a flow field with high turbulence and large temperature differences. These thin film cooling flows provide a good test case for evaluating computational model prediction capabilities. The goal of this work is to provide a database of flow field measurements for validating computational flow prediction models applied to turbulent heat transfer flows. In this work we describe the application of a Dual-Plane Particle Image Velocimetry (PIV) technique in a thin film cooling wind tunnel facility where the injection air stream velocity and temperatures are varied in order to provide benchmark turbulent heat transfer flow field measurements. The Dual-Plane PIV data collected include all three components of velocity and all three components of vorticity, spanning the width of the tunnel at multiple axial measurement planes.

Introduction

Thin film cooling is an important phenomena used in many aspects of turbomachinery and in rocket propulsion (Refs. 1 and 2). The applications range from cooling turbine blades to cooling combustor liners. In all of these applications, a thin barrier of cool air is used to protect the underlying metal surfaces from the hot combustion gases in the freestream flow. These cooling films are typically generated by using a series of perforated holes in the substrate through which the cooling air is injected into the flow. The cooling air can be considered jets in cross flow and these jets interact with one another to make up the thin film. The turbulent momentum and heat transfer occurring in these flows is complex and difficult to accurately model using computation fluid dynamics.

NASA is interested in acquiring benchmark data on thin film cooling flows for use by computational fluid dynamics code developers for assessment of their turbulence models in these complex turbulent flow fields involving heat transfer. Both the mean flow and turbulence statistics are required for this assessment. While such data exist for unheated cases and simple geometries, there is a lack of sufficient data for flows where thermal mixing and/or heat transfer are the key flow phenomena. This is a multi-facetted project where temperature and velocity fields are to be measured. Here we only discuss the flow measurement aspect using Particle Imaging Velocimetry (PIV).

A small scale wind tunnel specifically designed for studying thin film cooling was used in this work (Refs. 3 and 4). Traditionally, probe type surveys were used to characterize the tunnel flow. However, in this study, to eliminate interferences caused by the insertion of the probe body, the non-intrusive PIV technique was used. Instead of the more traditional PIV, the Dual-Plane PIV technique is employed in order to obtain all three components of velocity and all three components of vorticity at different cross-stream planes with respect to the main flow direction (Refs. 5 and 6). Results from the processed Dual-Plane PIV data are presented for two different thin film cooling models at different flow conditions and different temperatures of the injected air stream. This document serves as an overview guide to researchers interested in using these flow measurements to validate Computation Fluid Dynamics (CFD) code predictions.

Approach

Particle Image Velocimetry is a widely used tool across a broad range of engineering disciplines. Here at NASA GRC, we have used PIV over the past 20 years in a wide range of applications including axial and centrifugal compressors, pulse detonation engines, supersonic parachute flows, jet plume/shock interactions, aeroacoustics, launch abort systems testing, mechanical heart valves, chicken embryo blood flow and microgravity flows. The CFD modelers are interested in as many properties of the flow field as can be measured in order to assess the fidelity of their computer model predictions and the underlying turbulence models. While we have previously applied Stereo PIV in thin film cooling flows (Ref. 7) (see acknowledgements in Ref. 7), for this application we chose to implement a more rigorous Dual-Plane PIV technique. In addition to all three velocity components across a plane, Dual-Plane PIV also provides all three components of the vorticity and all 9 elements of the Reynolds Stress Tensor, key flow quantities of interest to CFD modelers. As a computational fluid dynamics benchmark data set, we are not interested purely in thin film cooling—but actually more interested in the turbulent behavior generated by injected cooling flow. We modified the operating conditions of the rig to provide the maximum temperature differences to provide a good CFD modelling challenge. Both a single hole and three hole floor plate models were tested in order to provide single isolated jet flow and also to provide an interacting jet flow.

Thin Film Cooling Rig

As stated earlier, a small scale wind tunnel facility with a temperature controlled coolant loop was used to simulate the complex, highly three-dimensional flow field anticipated in thin film cooling flows (Ref. 3). The test section is specifically designed to be reconfigurable, accepting various floor plate and injection port arrangements. Two interchangeable, 30x scale air injection hole plates were used in this work: a three hole configuration to study interacting jets and a single hole configuration which is a more fundamental case since the jet is isolated in the center of the tunnel and has no interaction with adjacent injection plumes. The tunnel consists of an aluminum bellmouth, flow conditioning screens, and an acrylic test section, illustrated in Figure 1. For the PIV test, the side walls of the tunnel were fitted from floor to ceiling with 3 mm thick glass windows in order to provide optical access for the PIV system and transmission of the high pulse energy laser sheets.

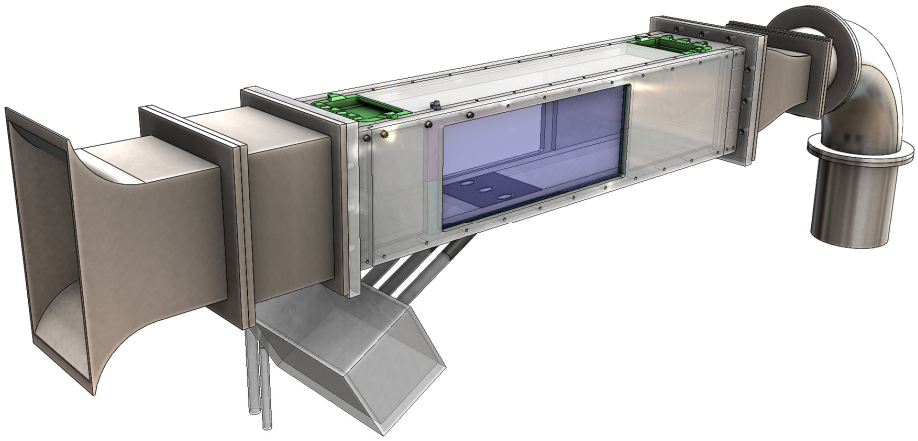

Figure 1.—Rendering of SW-6 facility showing the flow seeding mixing manifold below the tunnel test section and the 3-hole floor insert.

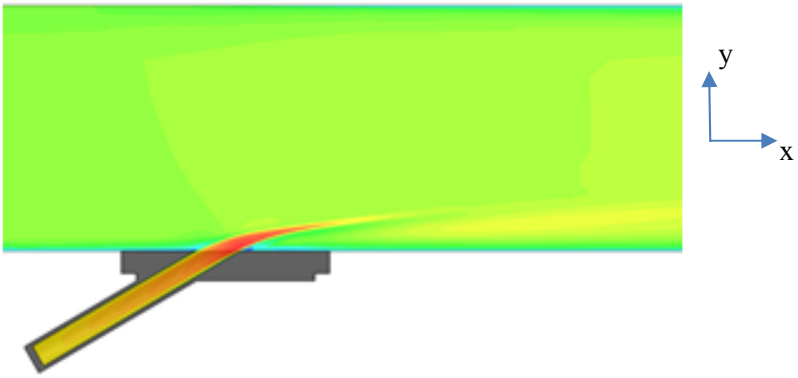

Figure 2.—Side view of the injection tube floor insert geometry with a CFD representation of the injection plume flow.

The two model test configurations were achieved by using a flat plate insert in the tunnel floor. A side view of the floor plate geometry for the test is shown in Figure 2. The air injection floor inserts were made out of ABS plastic using a 3D printer. The air injection holes on the 3-hole plate were inclined at 30° relative to the x-axis and had a z-axis hole diameter of D = 19 mm and a spacing of z/D = 3. Due to the oblique incidence, the elongated diameter of the hole along the flow direction (x-axis) was 38 mm. Perspective views of the tunnel floor plates are provided in the data results plots of Figures 5 and 9. The single hole floor plate had a hole diameter of 19 by 38 mm which was centered in the plate. In order to determine the tunnel flow rate, a total pressure probe was placed upstream of the test section and static pressure taps were placed on the sidewalls. Freestream temperature was measured with an open-ball thermocouple located upstream of the holes near the total pressure probe. Coolant temperature was measured with open-ball thermocouples inside the coolant tubes.

The blowing ratio (BR) is the ratio of coolant mass flow rate per unit area to freestream mass flow rate per unit area. Airflow in the tunnel is provided by facility altitude exhaust. Setting the vacuum pressure at the diffuser of the tunnel sets the tunnel operating point. Air is drawn from the room and passing through flow conditioning sections prior to entering the test section. The freestream velocity was 9.2 m/s and the Reynolds number based on freestream velocity and coolant hole diameter was 11,000. The test section is a square cross-section measuring 20.7×20.7 cm and has a total length of 1.2 m.

In normal operating mode, coolant flow is provided by blowing pressurized air through a heat exchanger, consisting of a copper tube coiled inside an ice–water tank. The coolant is then fed through a manifold to three separate flow meters, and then into acrylic tubes with L/D = 20 which are connected to each cooling hole in the floor of the tunnel. However, for the CFD modelling effort reported here, we were interested in the largest ΔT that could be obtained. So instead of cooling the injection air, it was heated using two 750W in-line electrical pipe heaters. With that in mind, we shall refer to the coolant flow as the injection air flow from this point forward. The injection air was heated to approximately 64 °C, providing a ΔT = 38 °C above the ambient air temperature in the tunnel. When operating with the single hole floor plate, the outside two tubes from the manifold were capped and all of the injected flow entered the tunnel through the center injection tube hole. The tunnel was operated at blowing ratios of 1 and 2 for the unheated cases and 1.15 and 2.3 for the heated injection air flow cases.

Dual-Plane PIV Technique

Stereo PIV is capable of providing all three components of velocity across the illuminated measurement plane. In order to maximize the information extracted from the turbulent heat transfer flow, we decided to implement the Dual-Plane PIV technique (Refs. 5 and 6). The Dual-Plane PIV technique consists of two stereo PIV systems that are focused on two separate, parallel light sheet planes which are closely spaced in the flow. Two dual-head, pulsed PIV type lasers with properly polarized beams are required in order to provide the requisite parallel plane illumination.

Polarization separation is used to isolate scattered light from the two stereo PIV systems since the 1st and 2nd exposures for both stereo PIV systems are occurring simultaneously. The light from the two different dual head laser systems are orthogonally polarized and then combined using a beam combiner module as shown in Figure 3. The Nd:YAG lasers used in this work produced vertically polarized beams with pulse energies of 200 mJ at a 10 Hz repetition rate. Laser system #2 used a half wave plate ($\lambda/2$) to rotate the polarization of both laser pulses into *s*-polarized light (horizontally polarized). The *s*-polarized light from laser #2 passes straight through the thin film polarizer (TFP) in the beam combiner. The *p*-polarized light from laser #1 reflects off of the TFP at Brewster's angle. A slight angular misalignment between the *s*- and *p*-polarized beams is required in order to obtain two closely spaced, parallel light sheets in the tunnel test section. The laser beams pass through cylindrical and spherical lenses to yield a pair of 1 mm thick light sheets that are parallel and spaced 1 mm apart in the tunnel test section. The light sheets exit the tunnel through the window in the back wall and are directed into a beam dump in order to minimize flare light.

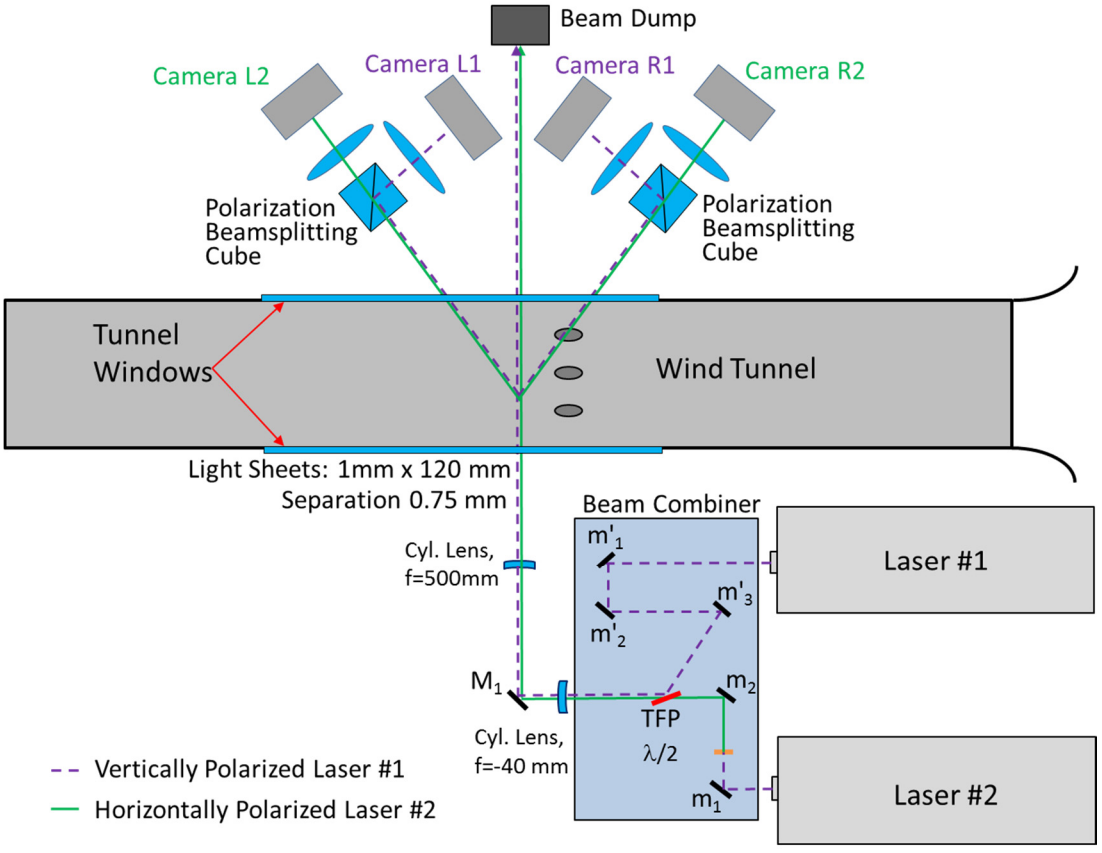

Figure 3.—Schematic layout of laser sheet polarization, beam combining module and Dual-Plane PIV system. Both lasers output at 532 nm. The purple colored, dashed laser beam is used to delineate the vertically polarized beam paths, compared to the horizontally polarized solid green beam.

The stereo PIV cameras image the orthogonally polarized light sheets through polarizing beam splitting cubes in order to achieve isolation of the two optical systems, see Figure 3. The stereo PIV cameras are mounted in Scheimpflug type mounts and are oriented at ±45° to the plane of the laser light sheet. The cameras view the light sheets from both sides of the sheets so that the cameras can be mounted on the same side of the tunnel and both cameras are in forward scatter mode. Stereo PIV system #1 (consisting of cameras L1 and R1) is sensitive to the *p*-polarized light from laser #1. Stereo PIV system #1's cameras view the reflected light from the polarizing beamsplitting cube and are oriented at right angles to the observation direction. Stereo PIV system #2 (cameras L2 and R2) is sensitive to the *s*-polarized light from laser #2's sheet which passes straight through the beamsplitting cube. Hence, although the laser light sheets are nominally 1 mm apart in the tunnel test section, each PIV system can only detect the light from its respective pulsed laser head. Also note that the PIV systems are configured in a "cross-stream" configuration, meaning the main flow direction is out of the plane of the light sheet.

The entire optical system is mounted on an optical breadboard which is in turn mounted on a dual parallel stage traverse system. The axis of the traverse system is aligned with the axis of the wind tunnel and also level with the floor of the tunnel. The traverse system enables the measurement plane of the PIV system to be traversed from 50 mm upstream of the floor plate injection hole axial center to 150 mm downstream. PIV measurement planes are initially acquired at 25.4 mm spacing until the center of the injection holes is reached and then the measurements are spaced in 6.35 mm increments.

The PIV cameras were mounted in a Scheimpflug configuration, where the tilt of the camera sensor relative the camera lens enables a tight focus on the particles across the obliquely viewed plane of the laser sheet. The 2048×2048 pixel PIV cameras were equipped with 50 mm lenses in order to achieve a nominal 100×200 mm field of view spanning the width of the tunnel. In addition, each camera is fitted with an electromechanical shutter in between the camera lens and the CCD sensor. The shutter enables the cameras to be operated at 5 Hz, while the PIV lasers are operated at their optimal pulse repetition rate of 10 Hz. The electromechanical shutters also help to reduce the exposure time down to 12 ms on the frame-straddled PIV cameras. All 4 cameras used in the Dual-Plane setup were controlled by a single computer system connected to two camera control units. Both of the laser systems were triggered at the same time so image acquisitions from the two stereo PIV systems were synchronized. Simultaneous acquisition of the flow properties at the two illuminated planes in the flow is required in order to compute the cross-plane flow properties. Each stereo camera pair was connected to one camera control unit. The computer was equipped with two framegrabbers, each connected to one camera control unit in order to acquire the images from all 4 cameras and stream them directly to disk in real time. Image sequences of 400 image pairs were acquired for each axial station. The processed Dual-Plane PIV data sets were configured with the origin of the coordinate system located at the leading edge of the center hole in the floor plate. PIV data were acquired at a total of 25 axial stations, starting from –31 mm upstream to +144 mm downstream from the injection hole leading edge.

The two independent stereo PIV systems were calibrated using a dual sided, dual plane calibration target, which was mounted on the PIV system traverse base plate below the tunnel. The calibration target projected up inside the tunnel test section by removing all of the tunnel floor plate inserts. The target was aligned with the laser light sheets. The PIV system traverse was scanned to each measurement station and a set of calibration images were acquired. Calibrations were performed for each axial measurement station to account for any variations in the wind tunnel windows or the elevation of the PIV system cameras. In addition to performing calibrations to a 3rd order polynomial, a calibration verification operation was performed to ensure that the calibration plane was accurately aligned with the laser light sheet plane (Ref. 8).

The PIV image data were processed using multi-pass correlations with 64×64 pixel subregions on 32 pixel centers, followed by 16×16 pixel subregions on 8 pixels centers. Subregion distortion processing was also used to process the PIV data (Ref. 9). Subregion distortion was used to correct for velocity gradients across the subregion and to minimize the "peak-locking" effect, which is the tendency for the estimated particle displacements to preferentially concentrate at integer values. In the subregion distortion

technique, the local velocity gradients surrounding the current correlation subregion are used to distort the subregion before the cross-correlation processing operation. Distorting the subregion yields correlation subregions with uniform particle displacements, and hence, reduces any bias caused by the velocity gradients. Typically two additional passes after the multi-pass processing are used with subregion distortion applied to refine the correlation peak estimates. The Left and Right vector maps were then processed using an in-house code to obtain the 3D vector maps. The final cross-stream velocity vector maps had 1.4 mm spatial resolution. Sequences of 400 velocity vector maps were acquired at each measurement station and ensemble averaged to provide first and second order statistics over the entire measurement plane. Chauvenet's criteria was used to eliminate any outliers in the ensemble averaging process (Ref. 10).

The ensemble averaging step was also the point at which the data from the two laser light sheets were used to compute the cross-plane flow vorticity, which is the unique aspect of the Dual-Plane configuration. Vorticity was computed on each instantaneous velocity vector map and then the instantaneous vorticity was ensemble averaged to yield the final vorticity estimates. Although two measurement planes were acquired, the data written out were only for a single plane, including the out of plane vorticity component estimates.

Accuracy of the Measurements

The error in estimating the velocity is determined by the accuracy by which the correlation peak location can be measured. Nominally the error in estimating the correlation peak is ±0.1 pixels. The full scale particle displacements for this flow were nominally 6 pixels in the injected air plumes and 2.5 pixels in the main tunnel flow. The relative error in the injection plume displacements (which is equivalent to velocity), is then σ_u = 0.1 pixels/6 pixels = 0.016. The relative error in the main tunnel velocities is σ_u = 0.1 pixels/2.5 pixels = 0.04. When we compute the ensemble average velocity estimates we further reduce the error in velocity by $1/\sqrt{400}$. Hence, the PIV velocity data reported here have an accuracy of better than 1 percent throughout the flow field.

Flow Seeding

In order for the Dual Plane PIV technique to work, we are relying on polarization separation to isolate the optical systems. A crucial requirement in any polarization isolation system is the seed particle size. If the particles are too large, then the scattered light will be depolarized and both optical systems will see the scattered light from both lasers, thereby cross-contaminating the recorded particle images. Particles less than 1 μm in diameter preserve the polarization state of the incoming light. Hence, we have a strict requirement that the seed particles used in the experiment must be less than 1 μm in diameter.

Both the main tunnel flow and the injected flow streams were independently seeded. For the main tunnel flow we used a six jet atomizer, which is based on the Laskin nozzle design. When filled with olive oil, this seeder provides particles with a mean diameter of 0.7 μm.

The concentration of seed particles generated by the 6-jet seeder have to be diluted before entering the tunnel in order to avoid locally high concentrations of seed particles. In order to homogenize the seeded air entering the tunnel, the seeder was placed inside a 0.8×1.0×1.0 m box positioned approximately 0.5 m upstream from the bellmouth inlet of the tunnel. The end face of the box closest to the tunnel inlet was covered with a metal perforated plate, with about 50 percent open area. The end of the box facing away from the tunnel was completely open. A small muffin style fan was also placed in the box, pointed away from the tunnel inlet, in order to mix/disperse the seed emanating from the 6-jet seeder with the ambient air. When the tunnel was operating, air was drawn through the seeder mixing chamber into the tunnel bellmouth providing well mixed, uniform seeding inside the tunnel.

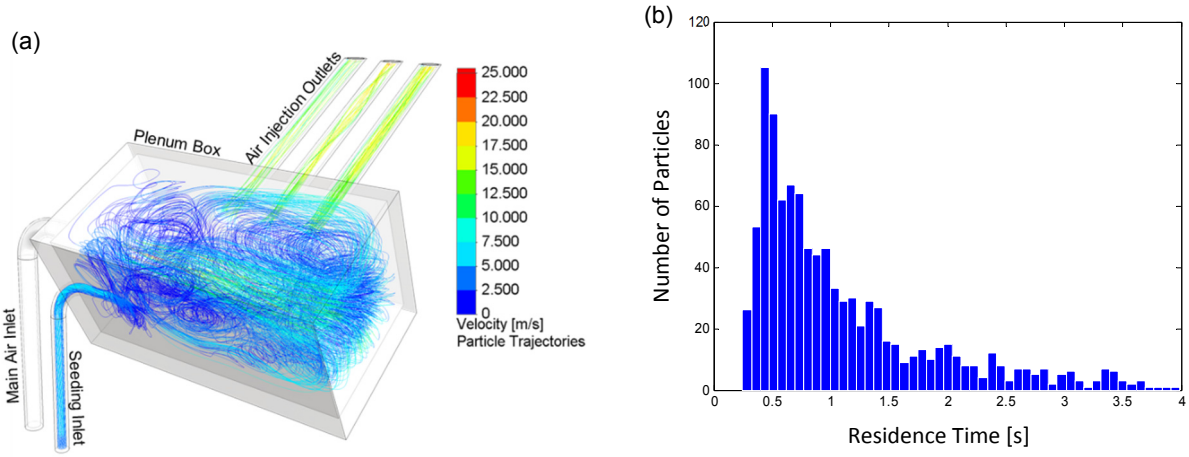

Figure 4.—(a) CFD prediction of the air supply and seed streams entering the manifold below the tunnel, where the streamlines indicate the path of the seeded air stream; (b) Histogram of the particle residence times inside the manifold.

The injected air flow was seeded using a single jet Laskin type atomizer also filled with olive oil. The effluent from the single jet atomizer was fed into a manifold below the tunnel. This manifold provided the pressurized air to all three of the injection tubes. The pressure line to the single jet seeder was adjusted to provide the desired seeding level in the injection air streams, as confirmed by visual inspection of the seeding level illuminated by the laser light sheet in the tunnel. The amount of seed material required to seed the injected flow was less than 1 percent of the total flow rate. An initial seeding configuration was used where the air supply to both the seeder and the mixing manifold were both fed through a single flow meter. The total flow rate for the injection air stream remain unchanged whether the seeder was turned on or off, confirming the contribution of the seeder flow on the total flow rate was negligible.

Prior to the initial testing of the seeder system, several CFD studies where performed to estimate the mixing performance of this injection port plenum. Historically, the success of a PIV measurement campaign is tightly coupled to the seeding quality, so predicting this performance is more insightful than the more traditional trial and error approach. Based on the seed particle mixing CFD predictions, seed injection uniformity and seed residence time in the plenum was considered acceptable. Figure 4 illustrates a sample case of this analysis. Figure 4(a) on the left visualizes the predicted particle trajectories to quantify the seed uniformity at the inlet of each individual injection port. Figure 4(b) contains a histogram plot of particles' residence times in the manifold to ensure excessive recirculation zones, where oil droplets may agglomerate into >1 μm in diameter, are minimized.

Results and Discussion

The Dual Plane PIV system was used to collect data on both the 3-hole and single hole floor insert models. Blowing ratios of 1 and 2 were covered. Both heated and unheated injection air streams were tested. With the electric heaters turned on, the injected air stream was approximately 64 °C. Nominal blowing ratios of 1.0 and 2.0 were obtained with no heat and with the heaters turned on the blowing ratios were nominally 1.15 and 2.3. The origin for all of the flow measurements was centered on the tunnel floor at the leading edge of the center injection port. The PIV data were collected starting at x = –31 mm upstream of the injection port leading edge. The second plane was acquired at x = –6 mm upstream of the hole leading edge. All subsequent measurement stations were acquired starting at +19 mm from the hole leading edge in increments of 6.35 mm to a distance of 144 mm downstream from the leading edge of the holes. The data sequences collected contained 400 image planes per stereo PIV system. The data were processed as described in the data processing section and combined into a single data set containing the mean u-, v- and w-components of velocity and the x-, y- and z-components of vorticity. The u'v', u'w' and v'w' Reynolds stresses were also computed. All of the data from the 25 measurement planes were combined into a single

block of data which is in Tecplot format. The spatial resolution of the in-plane measurements is 0.7 mm, or y/D = z/D = 0.037. All of the measured flow field quantities and physical dimensions were made dimensionless using the injection port diameter D and/or free stream tunnel velocity U_∞.

The PIV measurements do not span all the way to the floor or to the tunnel walls. There is always flare light scattered from surfaces when light travels through glass that is not anti-reflection coated. The flare light precludes our ability to perform the cross-correlation operation near these surfaces. We also had to take additional preventative measures to keep the light sheet from intersecting the tunnel floor. We could not simultaneously collimate the light sheet and keep the two light sheets parallel through the test section with the optics we had available, therefore we had to block the light sheet further above the floor on the near side of the tunnel to keep the diverging sheet from illuminating the floor on the far side of the tunnel.

The mean flow velocity magnitude is plotted in Figures 5 to 12 for each model and test configuration. There are two plots for each test condition: (1) a streamwise plane with velocity vectors and an iso-velocity contour depicting the edge of the air injection plume and (2) a cross-stream contour plot of velocity magnitude at x/D planes of 2, 3, 4, and 5. For the 3-hole model configuration, the nominal BR = 1.0 case is shown with room temperature air and then heated air, which is followed by the nominal BR = 2.0 case with unheated and then heated air. Next, the 1-hole model results are plotted, again first for a nominal BR = 1.0 and then for a nominal BR = 2.0. The exact test matrix settings are summarized in Table 1. Note that the BR ratios are slightly elevated when the heaters were turned on due to the configuration of the volumetric flow meter relative to the heaters. The Experimental Configuration Name column is how the data was designated in the PIV notebook and also how the processed PIV data are organized on the archival DVD.

The 3-hole model cases show that there is some minor interaction of the central plume with the plumes on either side, as evidenced by the asymmetry in the two outside plumes in the cross-stream plots. Secondly, regardless of the model, the velocity in the injected plume tends to have approximately 20 percent higher velocity and penetrates approximately 20 percent further into the freestream flow for the heated plume cases when compared to the cold-flow cases. The decreased density of the heated injection air is responsible for this further penetration into the freestream tunnel flow. The velocities of the injected plume are higher due to the reduced density of the injection air. Maintaining the same mass flow for the heated case requires increasing the velocity of the injected air in order to compensate for the reduced air density. Some of the non-uniformities observed in the peripheral regions of the tunnel are partially due to the mismatch in some of the tunnel floor inserts and the different sub-sections of the tunnel that are bolted together. The 3D printed model parts exhibit a small degree of warping after being printed, causing some of the mismatch. Since different model configurations were tested over several days, smoothing out the interfaces between the tunnel inserts was not feasible. Overall, we do not expect these small disturbances in the flow to significantly influence the injected plume/free stream interaction.

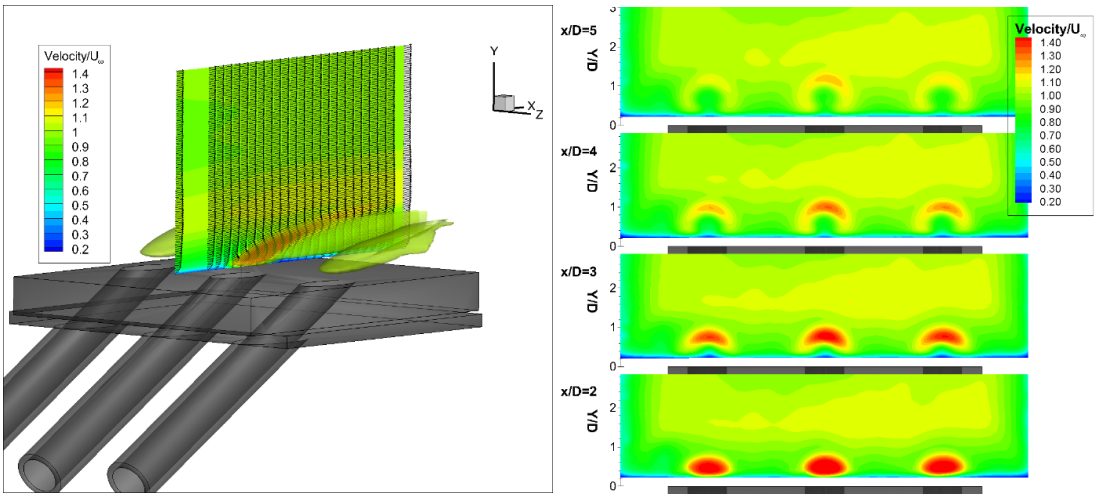

Figure 5.—Streamwise and cross-stream velocity for 3-hole floor model, blowing ratio of 1.0 and no heat.

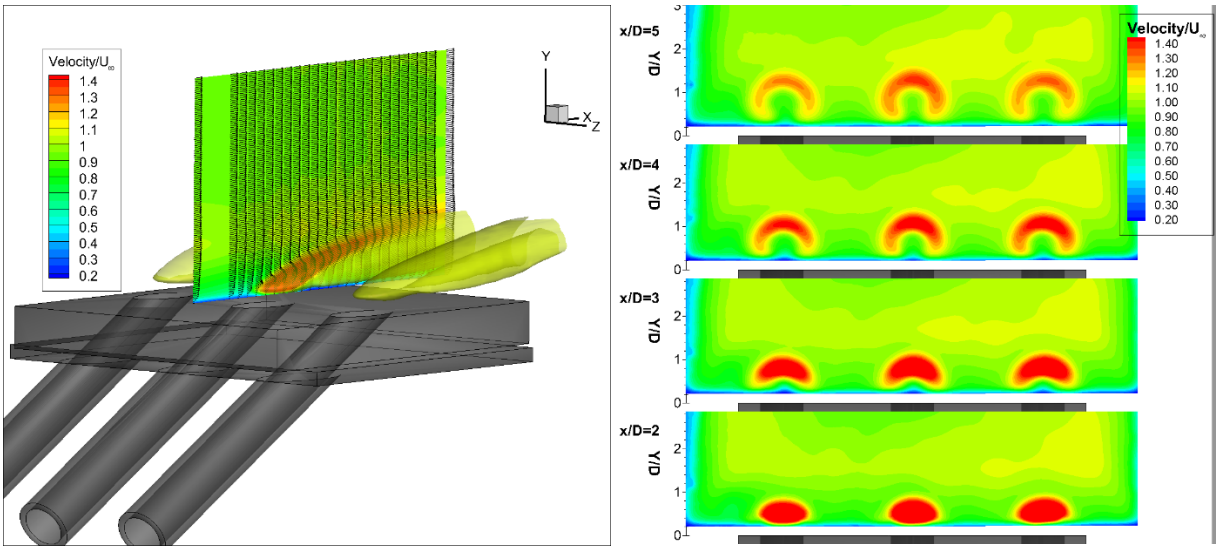

Figure 6.—Streamwise and cross-stream velocity for 3-hole floor model, blowing ratio of 1.2 and with heat.

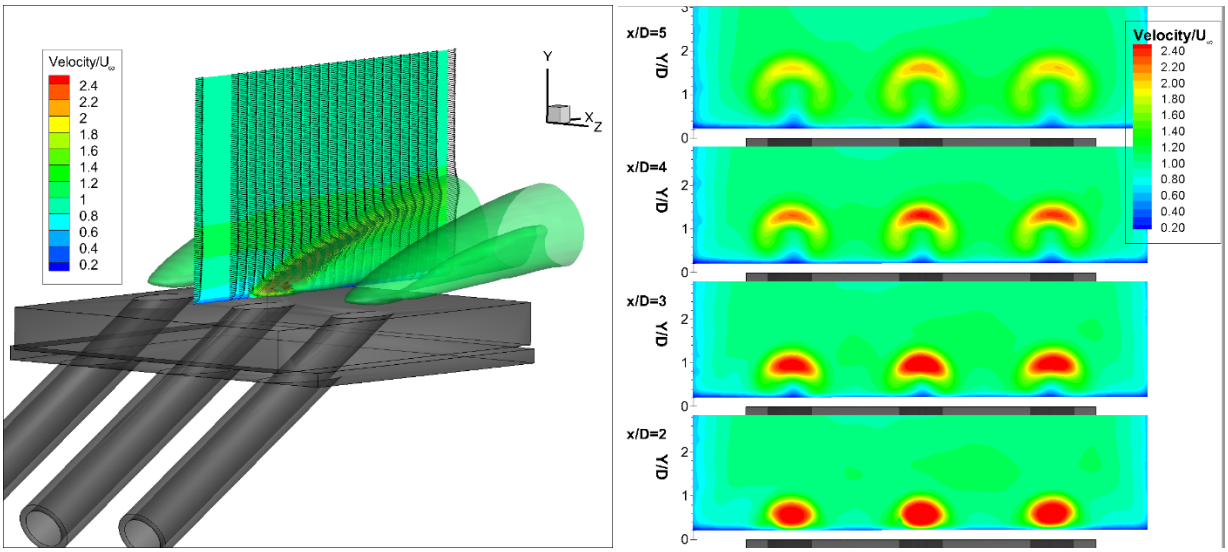

Figure 7.—Streamwise and cross-stream velocity for 3-hole floor model, blowing ratio of 2.0 and no heat.

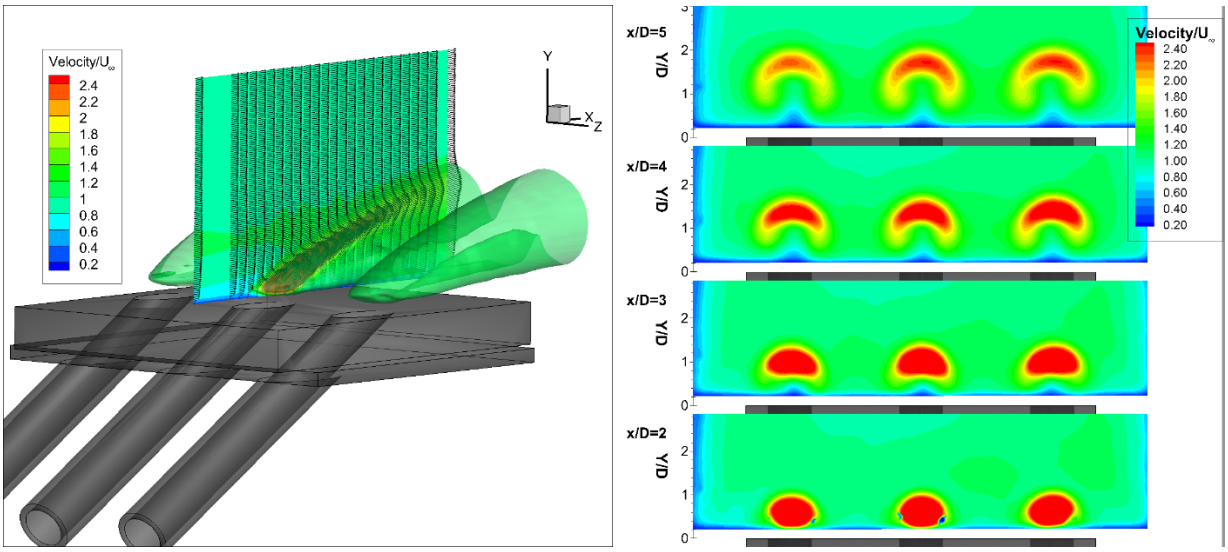

Figure 8.—Streamwise and cross-stream velocity for 3-hole floor model, blowing ratio of 2.3 and with heat.

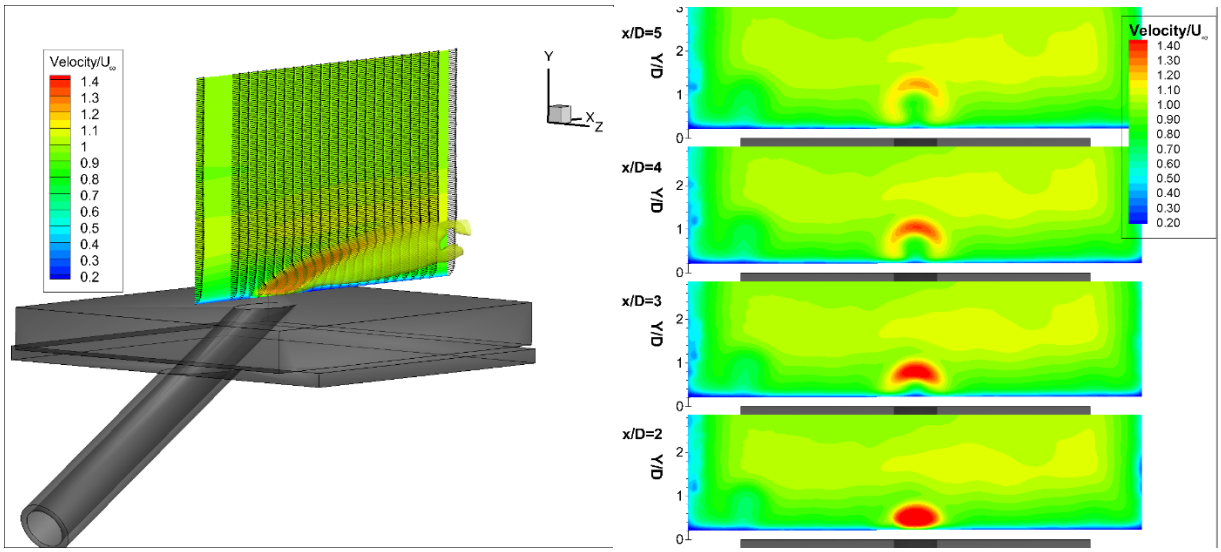

Figure 9.—Streamwise and cross-stream velocity for 1-hole floor model, blowing ratio of 1.0 and no heat.

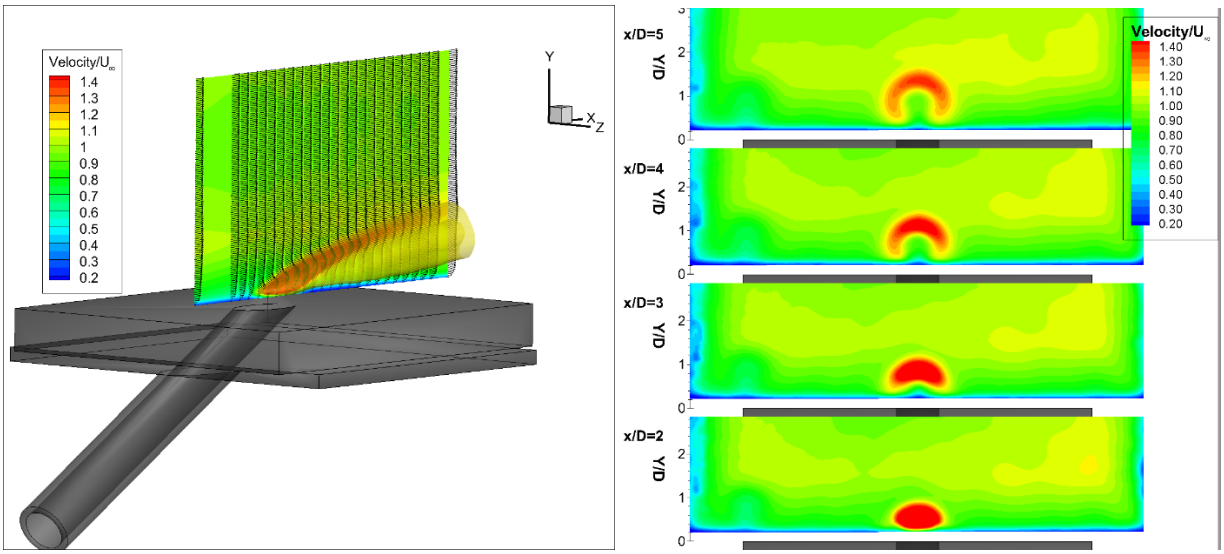

Figure 10.—Streamwise and cross-stream velocity for 1-hole floor model, blowing ratio of 1.1 and with heat.

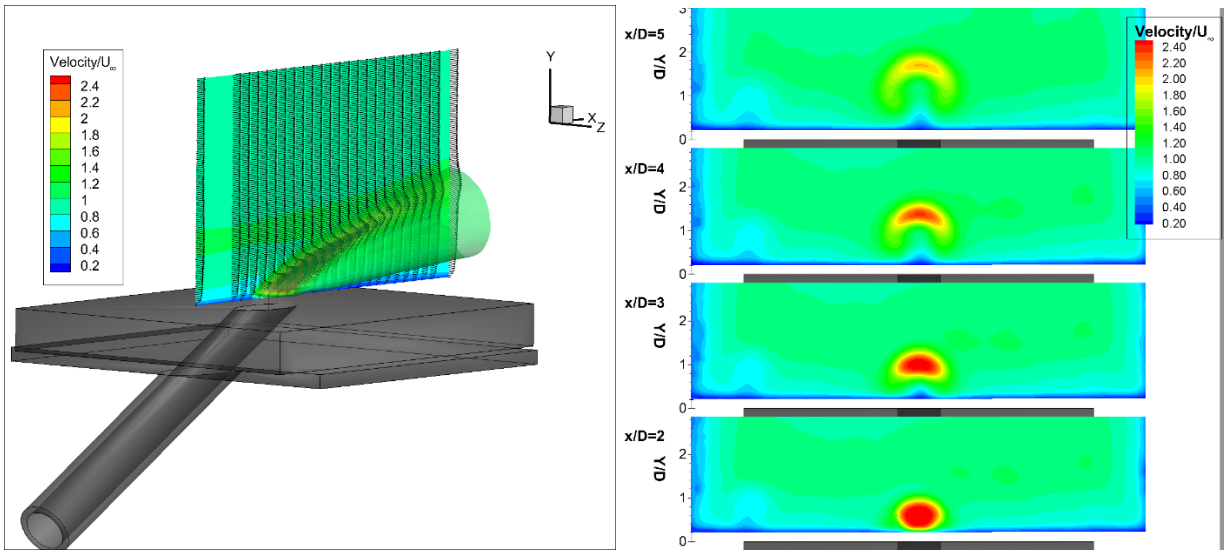

Figure 11.—Streamwise and cross-stream velocity for 1-hole floor model, blowing ratio of 2.1 and no heat.

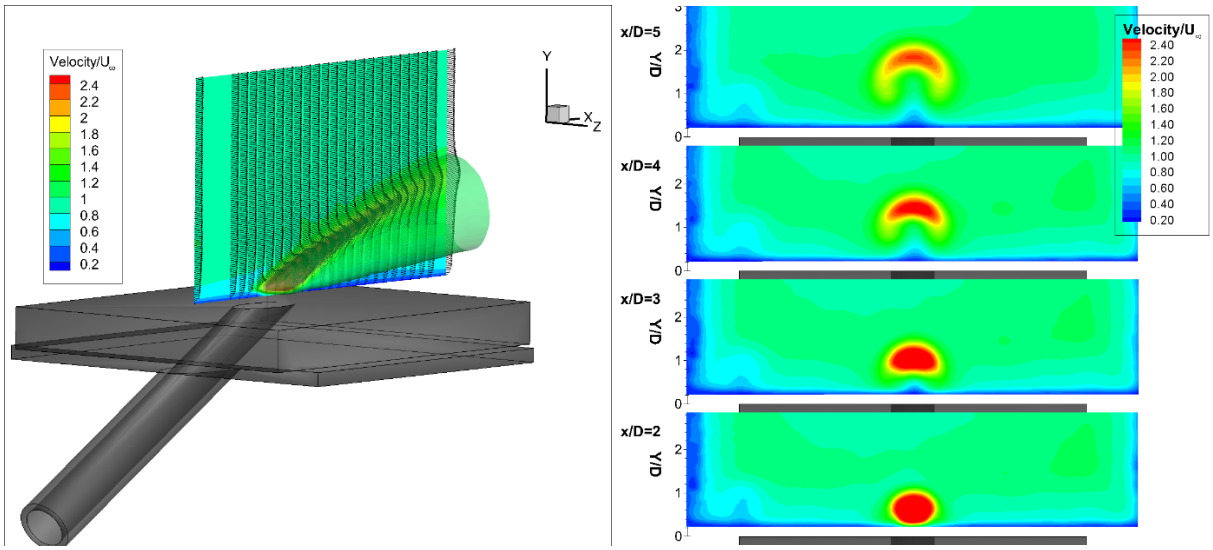

Figure 12.—Streamwise and cross-stream velocity for 1-hole floor model, blowing ratio of 2.3 and with heat.

TABLE 1.—TEST MATRIX CONDITIONS AND CONFIGURATIONS

Experiment configuration name	Model	V_{Tunnel} [m/s]	ρ_{Tunnel} [kg/m^3]	$V_{Injection\ Air}$ [m/s]	$\rho_{Injection\ Air}$ [kg/m^3]	$T_{Injection\ Air}$ °C	Blowing ratio
21Oct15a	1-Hole	9.2	1.16	19.0	1.16	26	2.1
21Oct15b	1-Hole	9.2	1.16	9.5	1.16	27	1.0
21Oct15c	1-Hole	9.2	1.16	23.9	1.03	64	2.3
21Oct15d	1-Hole	9.2	1.16	11.9	1.03	64	1.1
20Oct15a	3-Hole	9.2	1.17	18.8	1.16	25	2.0
20Oct15b	3-Hole	9.2	1.17	9.4	1.16	25	1.0
20Oct15c	3-Hole	9.3	1.17	24.0	1.03	64	2.3
20Oct15d	3-Hole	9.1	1.17	12.0	1.03	63	1.2

A sample cross-stream plot of velocity vectors on top of color contours of velocity magnitude is shown in Figure 13, which demonstrates the spatial resolution of the data. The details of the bound vortex pair development in the injection plume are clearly evident. Furthermore, the depth of information contained in the Dual-Plane PIV data set is demonstrated in Figure 14, where a series of cross-stream plots of all three components (ω_x, ω_y, ω_z) of vorticity are shown. The vorticity is made dimensionless by scaling the data by the hole diameter D and the tunnel free stream velocity U_∞. The in-plane vorticity, ω_x is a common flow quantity easily computed from standard single-plane stereo PIV data. In Figure 14(a), we see the plot of ω_x (out of the measurement plane) which clearly shows the roll up of the flow under the bound vortex pair. In Figure 14(b), the plot of ω_y illustrates the mixing along the sides and in the interior of the high speed injection plume with the ambient tunnel flow. Lastly, in Figure 14(c), the plot of ω_z shows the interaction of the top and bottom edges of the high speed jet plume with the ambient tunnel flow. Figure 14 demonstrates the information gained by using Dual-Plane PIV, where in addition to the standard out-of-plane vorticity, we are able to compute both of the in-plane vorticity components.

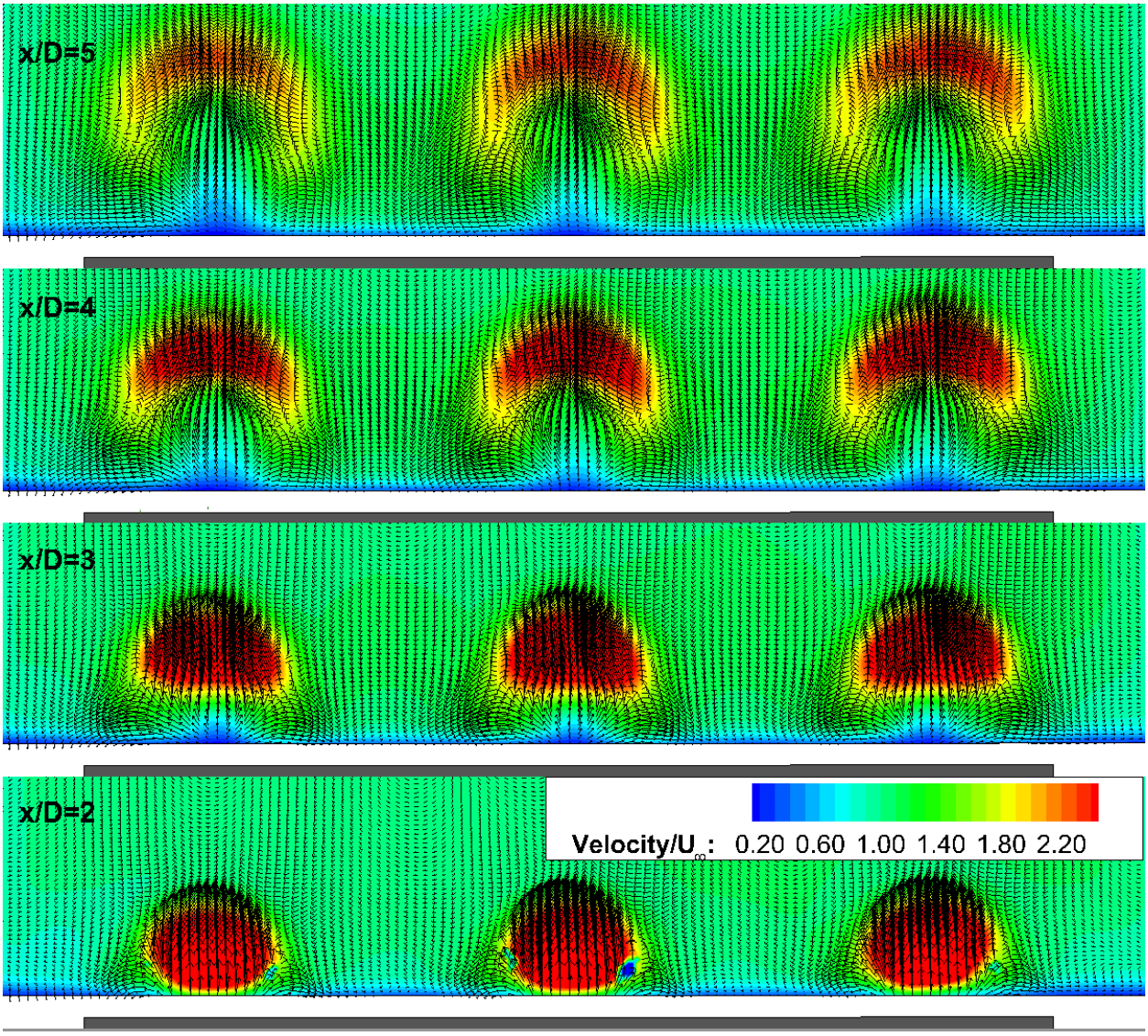

Figure 13.—Plot of the velocity vector files on top of the velocity magnitude contours for the 3-hole model case with a blowing ratio of 2.3 and heated injection air. Every other column of vectors are plotted for clarity.

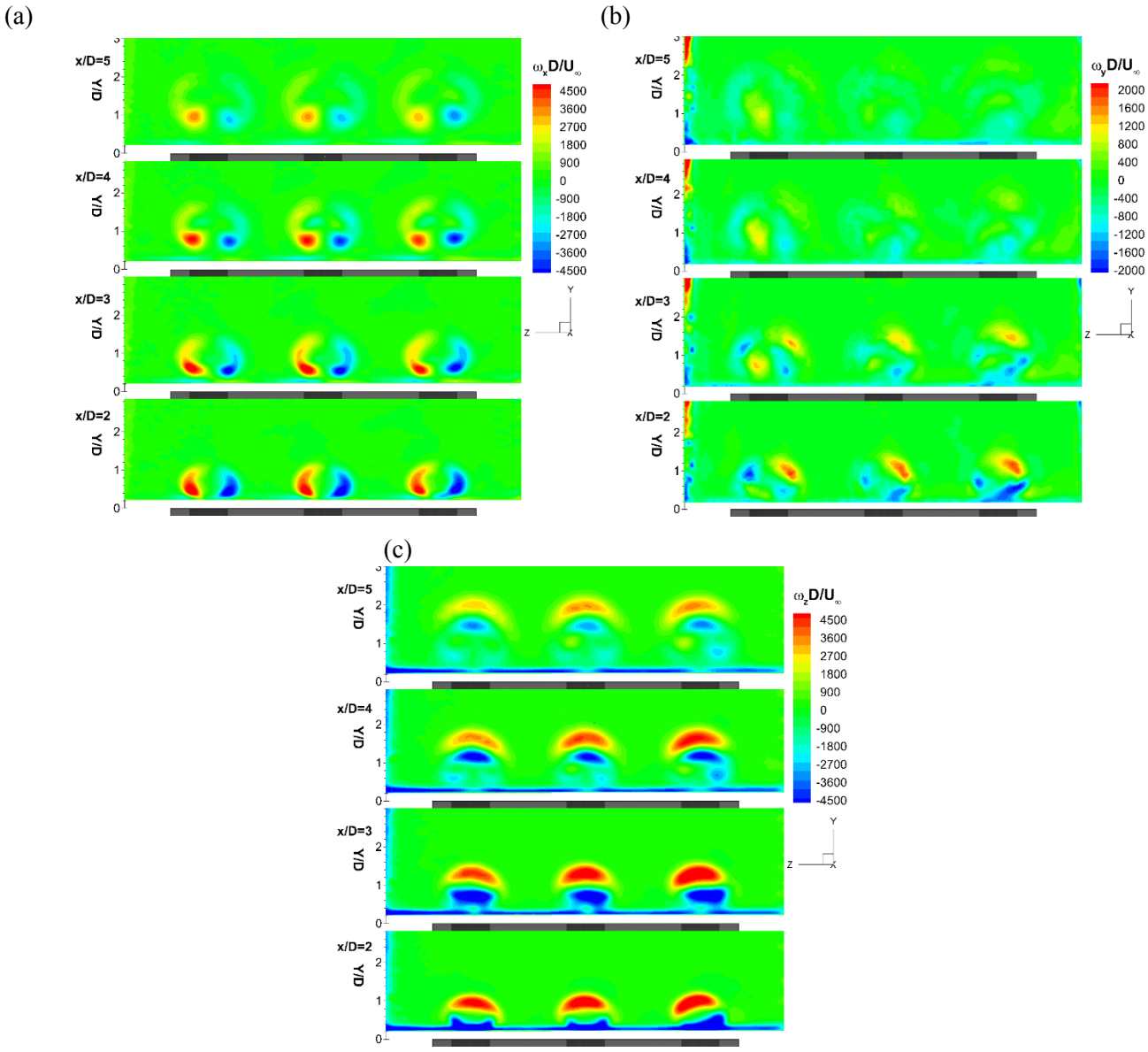

Figure 14.—Here we show all three measured components of vorticity for a blowing ratio of 2.3 with heat: (a) ω_x, (b) ω_y, (c) ω_z. Measuring all three components of vorticity across a plane is a rarely demonstrated measurement capability.

Conclusions

Dual-Plane PIV has been successfully applied in a low speed wind tunnel for studying turbulent heat transfer flow fields. The PIV data were acquired using both a 3-hole and single hole floor plate models installed in the wind tunnel. Two blowing ratios were measured for each model. Both ambient temperature and heated air were injected into the main tunnel flow. The development of the horseshoe vortices in the classic jet in cross-flow configuration is readily observed in the PIV data. The penetration of the jet plume into the tunnel freestream flow increases with temperature. In addition to the standard in-plane flow quantities, the application of the Dual-Plane PIV technique enables the computation of out-of-plane flow quantities so that all three components of vorticity are measured. The data collected here are of high spatial resolution and high accuracy providing a benchmark set of conditions for validating CFD predictions on turbulent heat transfer flows.

Postnote

The polarizing beamsplitting cubes were an essential element in the Dual Plane PIV used in this test program. However, the polarizing beamsplitting cubes did not perform as well as desired. The large field-of-view requirement of the PIV systems exceeded the acceptance angle of the beamsplitting cubes resulting in small regions of the reflected images (vertically polarized light) seeing some the horizontally polarized scattered light. This small deficiency did not significantly affect our ability to make the velocity measurements. However, any future implementations of the Dual Plane PIV technique requiring the large field angles required here will employ wire grid polarizers in front of the PIV cameras for polarization isolation. The dual stereo system cameras will be mounted side-by-side and the small difference in the stereo PIV system viewing angles will be inconsequential in the data processing.

Post Postnote

The original TM has been revised to correct the exact blowing ratios that were used in the experiments and also to revise the PIV data processing. In the initial report, the volumetric flow rate was being used with additional pressure and temperature readings to compute the mass flow rate, which worked fine for the unheated cases. However, for the heated cases the change in air density was not taken into account and resulted in an under prediction of the mass flow in the tube. The correct blowing ratios for the heated injection air cases were actually 1.1 and 2.3, which are slightly higher than the unheated blowing ratio cases of 1.0 and 2.0. As an additional check subsequent to the PIV tests, a new mass flow meter was installed downstream of the heaters and used to verify the injection air mass flow estimates computed using the volumetric flow meters.

Further analysis of the PIV results and comparison with hot wire measurements and CFD predictions indicated that the PIV turbulence levels were much lower than expected. The PIV data were then reprocessed using smaller sized subregions (16×16 pixels) on an even finer grid (8×8 pixels). Application of these smaller subregions was possible due to the high seed particle concentration in the image data. The smaller sized subregions enabled recovery of more accurate turbulence levels, which had been low pass filtered using larger subregions sizes of 32×32 pixels on a 16×16 pixel grid as reported in the initial version of the TM. The PIV data now much more closely match the hot wire measurements and CFD predictions of the injection air flow field.

References

1. Garg, V.J., Gaugler, R.E., 1997, "Effect of coolant temperature and mass flow on film cooling of turbine blades," Int. J. of Heat Mass Transfer, Vol. 40, No. 2, pp. 435–445.
2. Golladay, R.L., 1967, "Gaseous-film cooling of a rocket motor with injection near the throat," NASA TN D-3836.
3. Shyam, V., Thurman, D., Poinsatte, P., Ameri, A.A., Eichele, P., 2014, "Long Hole Film Cooling Dataset for CFD Development - Flow and Film Effectiveness," AIAA–2014–3522, 50th AIAA/ASME/SAE/ASEE Joint Propulsion Conference, July.
4. Thurman, D.G., El-Gabry, L.A., Poinsatte, P.E., and Heidmann, J.D., 2011, "Turbulence and Heat Transfer Measurement in and Inclined Large Scale Film Cooling Array – Part II, Temperature and Heat Transfer Measurements," ASME paper GT2011-46498, ASME Turbo Expo 2011, Vancouver.
5. Kaehler, C.J., Kompenhans, J., 1999, "Multiple plane stereo PIV: technical realization and fluid – mechanical significance," Proceedings of the 3rd International Workshop on PIV, Santa Barbara, September 16–18.
6. Hu, H., Saga, T., Kobayashi, T., Taniguchi, N., Yasuki, M., 2001, "Dual-plane stereoscopic particle image velocimetry: system setup and its application on a lobed jet mixing flow," Exp in Fluids, 31, pp. 277–293.

7. Thurman, D., Poinsatte, P., Ameri, A.A., Culley, D., Raghu, S., Shyam, V., 2015, “Investigation of spiral sweeping holes,” GT2015-43808, *Proceedings of the ASME Turbo Expo 2015*, June 15–19, Montreal, Canada.
8. Bjorkquist DC (2002) “Stereoscopic PIV calibration verification,” Proceedings of the 11th international symposium on application of laser techniques to fluid mechanics, Lisbon, Portugal, July.
9. Scarano F. (2002) Iterative image deformation methods in PIV. Meas. Sci. Technol., Vol. 13, pp. R1–R19.
10. Taylor, J.R., An Introduction to Error Analysis, University Science Books, Oxford University Press, Mill Valley, CA., 1982, pp. 142–144.